Multiaxial fatigue criteria versus experiments for small crack under rolling contact fatigue

S. Foletti *, S. Beretta, M.G. Tarantino

Politecnico di Milano, Dipartimento di Meccanica, Via La Masa 1, 20156 Milan, Italy

Article history:
Received 8 April 2013
Received in revised form 11 May 2013
Accepted 19 May 2013
Available online 30 May 2013

1. Introduction

Multiaxial fatigue has been the subject for the proposal of many criteria intended to predict fatigue strength (or fatigue life) under multiaxial conditions from a limited number of tests under uniaxial or torsional conditions. Among the different multiaxial loads, the out-of-phase (OOP) conditions that are typical of rolling contact fatigue (RCF), both for subsurface and surface failures, are in general the most detrimental for mechanical applications, with a severe reduction of the allowable fatigue shear strength respect to simple torsion.

RCF is traditionally treated in terms of an allowable Hertzian pressure [1], while the Dang Van criterion [2] has been the theory widely adopted for several applications including RCF [3–5], due to the treatment of out-of-phase stress components histories and the simple definition of allowable shear stress, as a linear function of the hydrostatic stress σ_h. Nevertheless, fatigue failure assessments under RCF cannot be made regardless of the influence of small defects. Service life of high strength steel bearings is found to be affected by the presence of small inclusions whereas catastrophic failures of railway wheels are triggered by sub-surface defects [6]. Therefore, it is important to consider the presence of defects for a significant strength prediction under RCF conditions.

In the literature two typical treatments of RCF in presence of defects are adopted: (a) calculation of the stress intensity factor (SIF) at the tip of defects and by comparing it with the threshold stress intensity factor range, ΔK_{th}, obtained under Mode II/III [7,8] and (b) use of a fatigue criterion in which the fatigue limit depends on defect size by assuming, according to Murakami's concept, that defects can be treated as small cracks [9].

The approach (a) is more rigorous since it employs a threshold condition for crack propagation based on the threshold values $\Delta K_{II,th}$ (or $\Delta K_{III,th}$), which are obtained in shear/torsion tests and account for shear mode failure mechanisms. However, this approach is found to overestimate the real threshold under RCF conditions. As a matter of fact, the authors have presented a novel series of experiments on microcracked specimens subjected to out-of-phase loads, which have clearly shown that the threshold $\Delta K_{III,th}$ in RCF conditions (both for a gear and a bearing steel) is much lower than that under simple torsion [10,11], due to the crack opening caused by the severe plastic deformation and rubbing of crack lips. However, up to now there are no experimental results for applications like the railway wheels, where mild steels are adopted.

The approach (b), for which the fatigue limit depends on defect size, does not appear to be fully correct when applied to RCF problems. As a matter of fact, for materials containing defects, even when a multiaxial fatigue criterion is able to correctly predict the

* Corresponding author. Address: Politecnico di Milano, Via La Masa 34, 20158 Milan, Italy. Tel.: +39 02 2399 8629; fax: +39 02 2399 8202.
E-mail address: stefano.foletti@polimi.it (S. Foletti).

Nomenclature

LP	loading path
OOP	out of phase
p_0	maximum contact pressure
R	stress ratio
RCF	rolling contact fatigue
s	ratio between the fully reversed torsional fatigue limit and the fully reversed uniaxial fatigue limit
SIF	stress intensity factor
α	angle between the fracture plane and the critical plane
α_{DV}	Dang van material parameter
β, η, k	Liu–Mahadevan material parameters
kv	cyclic yield shear stress
Δa	coplanar crack depth
ΔK	stress intensity factor range
ΔN	number of cycle
$\sigma^H_{a,c}$	hydrostatic stress amplitude acting on the critical plane
$\sigma_{m,c}$	normal mean stress acting on the critical plane
$\sigma_{a,c}$	normal stress amplitude acting on the critical plane
σ_h	hydrostatic stress
σ_W	fully reversed uniaxial fatigue limit
$\tau_{a,c}$	shear stress amplitude acting on the critical plane
τ_W	fully reversed torsional fatigue limit
$\sqrt{area}$	crack size expressed in terms of square root of the projected crack area
$\sqrt{area_0}$	fictitious crack length parameter

Subscripts

I	Mode I
II	Mode II
III	Mode III
th	threshold
I,th,LC	Mode I threshold for long crack
III,th,OOP	Mode III threshold for out-of-phase loading

behavior of smooth specimens, it fails in describing the condition of non-propagating small cracks in presence of a high negative hydrostatic stress [12].

In the present paper we would like to address these two open points. Firstly, we present a summary of experimental results on very small defects under RCF conditions for two hard steels (respectively, a bearing and a gear steel), together with new results for a mild steel adopted for manufacturing railway wheels.

Then, the above experimental data are analyzed in terms of the criteria usually adopted in RCF applications (namely, Dang Van criterion [13,14] and Liu–Mahadevan criterion [15,16]). Finally, the conditions for the applicability of such criteria are discussed.

2. Experiments for Mode III thresholds in RCF

The materials tested for investigating Mode III crack thresholds under pure torsion and RCF conditions are two hard steel, a bearing steel and a Q&T steel for gears (SAE 5135 steel), and a ductile steel widely used for manufacturing railway wheels (R7T steel). Ultimate tensile stress (UTS) as well as monotonic and cyclic yield stress (0.2% plastic strain offset) are listed in Table 1.

As it can be observed, the three materials are very different in terms of monotonic and cyclic properties.

2.1. Specimen shape and dimension

All the fatigue tests were carried out onto micronotched hourglass specimens (Fig. 1). After machining, the specimens were hand polished and then electro-polished (surface removal 30–40 μm) in order to reduce the residual stresses.

After surface finish, artificial micronotches were then introduced onto the surface of the specimens by EDM machining: three different defects were introduced, characterized by a size (expressed in terms of Murakami's $\sqrt{area}$ parameter) of 220, 315 and 630 μm. Defect sizes are shown in Fig. 1.

2.2. Precracking and fatigue test details

All specimens were preliminary pre-cracking in Mode I in order to induce the formation of small non-propagating cracks at the bottom of the notches. The pre-cracking procedure was carried out under tension–compression, with a stress ratio $R = -2$ for 10^7 cycles, at stress levels slightly lower than the fully reversed uniaxial fatigue limit. After pre-cracking procedure all the specimens were observed under a scanning electron microscope (SEM) to verify the success of pre-cracking procedure, and if not successful, the Mode I loading was repeated. More details can be found in [10,11,17].

After the pre-cracking procedure, the specimens were subjected to torsional and out-of-phase tests at different Mode III stress intensity factor range, ΔK_{III}, values. The out-of-phase (OOP) tests were carried out according to three different load paths: in the case of the bearing steel, two load paths provided by SKF (the industrial partner) were adopted (namely load paths LP1 and LP2, which represent the stress state experienced by a sub-surface defect parallel and inclined in respect to the free contact surface respectively), while the gear and the railway steel were subject to a load path LP3, very similar to LP1. The three load patterns are shown in Fig. 2.

The tests were conducted in force/torque control using an MTS 809 Axial Torsional System. The surface-mixed mode crack advance was constantly monitored during the test by employing the method of plastic-replicas.

Following the fatigue test, all the specimens were examined under SEM, after having removed the debris clopping the defect, by intense ultrasonic cleaning in acetone. Both the specimen surface appearance and the co-planar (XZ plane in Fig. 1) fracture surface morphology were investigated (the latter inspected after static cryogenic rupture in liquid nitrogen). The coplanar crack growth rate was estimated at the end of each test as $\Delta a/\Delta N$, where Δa is the coplanar crack depth and ΔN is the number of cycles at the end of the test.

Table 1
Tensile properties of the three steels.

Material	UTS (MPa)	Monotonic yield stress (MPa)	Cyclic yield stress (MPa)
Bearing steel	2360	1980	2070
Gear steel	2150	1395	1735
Railway wheel steel	875	545	480

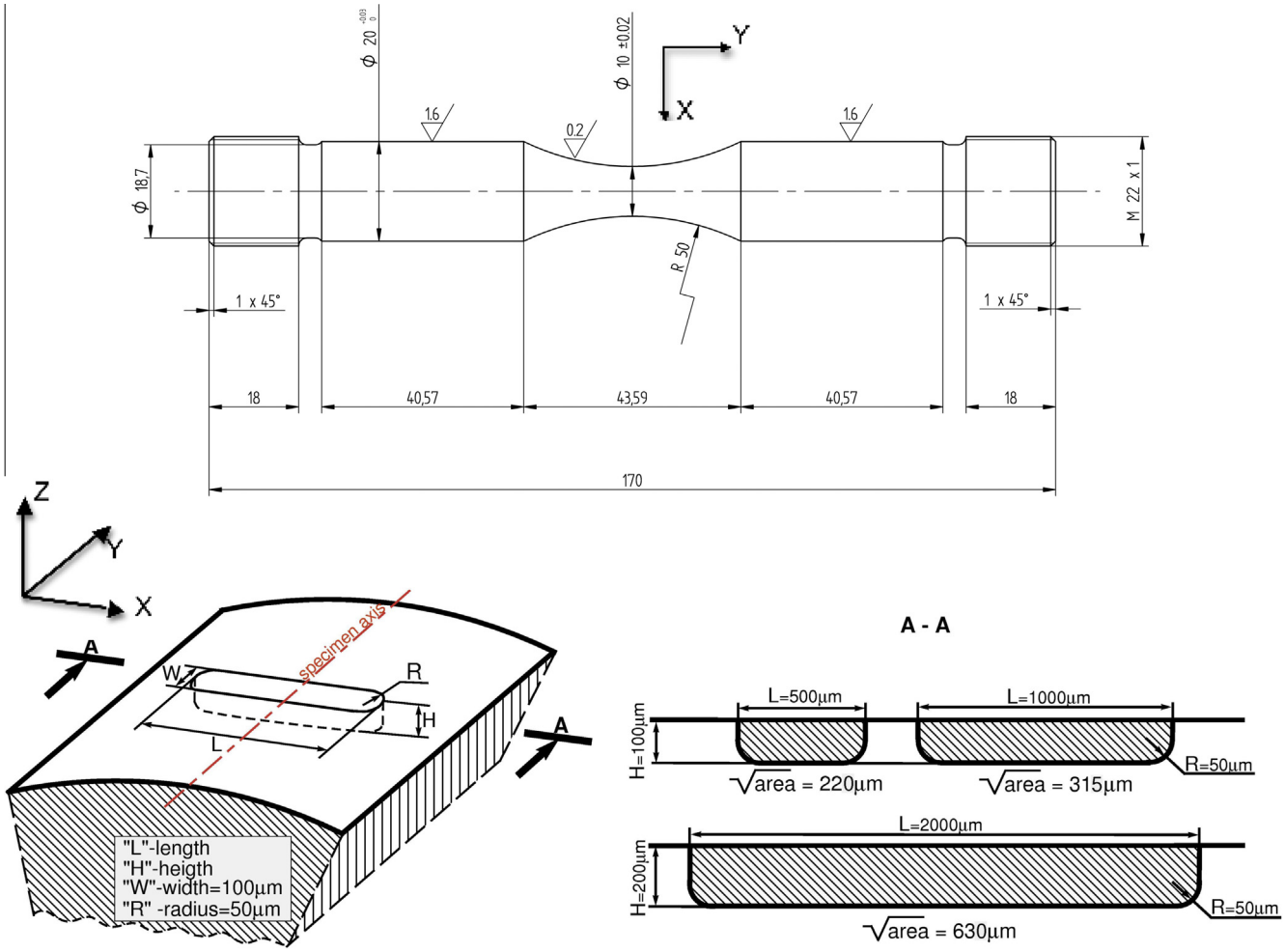

Fig. 1. Shapes and sizes of specimen and artificial micro-notches adopted in fatigue tests.

2.3. Fatigue test results

In the case of the bearing and the gear steel the crack growth under out of phase tests, LP1 and LP3 respectively, is found to be characterized by a co-planar shear growth (which correspond to a pure Mode II and Mode III at the surface point and at the defect tip respectively, see Fig. 3), accompanied by the formation of debris and plastic deformation of the crack mouth, at ΔK_{III} levels much lower than the ones corresponding to Mode I threshold.

For the same materials, tests under simple torsion showed a small co-planar crack advance (with a growth rate comparable to threshold region) at ΔK_{III} levels similar to $\Delta K_{I,th}$, together with the formation of pure Mode I cracks on planes tilted at 45° respect to crack plane, see Fig. 3. These Mode I cracks are the ones responsible for fatigue failure at stress levels higher than the fatigue limit and, correspondingly, the fatigue limit is the Mode I threshold onto the tilted cracks.

For the bearing steel, out-of-phase tests under LP2 show a behavior similar to torsion. The failure is controlled by Mode I propagation: the observation of fracture surfaces for interrupted tests reveals a small co-planar growth with the early development of Mode I on tilted planes, see Fig. 3. Details can be found in [17].

The experimental results on the railway wheel steel [18] reported in Table 2, fully confirm results onto bearing and gear steels. Two different defect sizes have been considered, characterized by a size (expressed in terms of Murakami's $\sqrt{area}$ parameter) of 220 and 630 µm. In Fig. 4, for each defect size, it is possible to note a huge and continuous coplanar crack propagation at a stress level much lower than the Mode I threshold for long cracks. The Mode III threshold under out-of-phase tests appears to be very low and can be estimate to be the 30% of the threshold for long crack, quite independently from the defect sizes.

Comparing this result with the previous ones obtained on different materials in terms of coplanar crack growth rate, $\Delta a/\Delta N$, as a function of the applied Mode III stress intensity factor, ΔK_{III}, normalized with respect to the Mode I threshold for long crack, $\Delta K_{I,th,LC}$ as reported in Fig. 5, it appears evident that it is always possible to note a strong reduction of the Mode III threshold under out of phase conditions ($\Delta K_{III,th,OOP}$). The major effect has been observed for the railway wheel steel, that is the more ductile tested material. Even if the entity of this reduction depends on material, the experimental results confirm the same failure mechanism for all the tested materials, characterized by plastic deformation and rubbing of fracture lips resulting in a residual opening between the crack lips. This is the reason why, for all the tested materials, it is always possible to note a strong reduction of $\Delta K_{III,th,OOP}$ in comparison to $\Delta K_{I,th,LC}$. During OOP fatigue tests the emission of debris, emerging from the crack, due to the abrasion process engendered by the interaction of the sliding rough crack surfaces during anti-plane shear, was noted.

3. Application of multiaxial fatigue criteria

The observed experimentally behavior, characterized by a strong reduction of allowable applied shear stress amplitude in

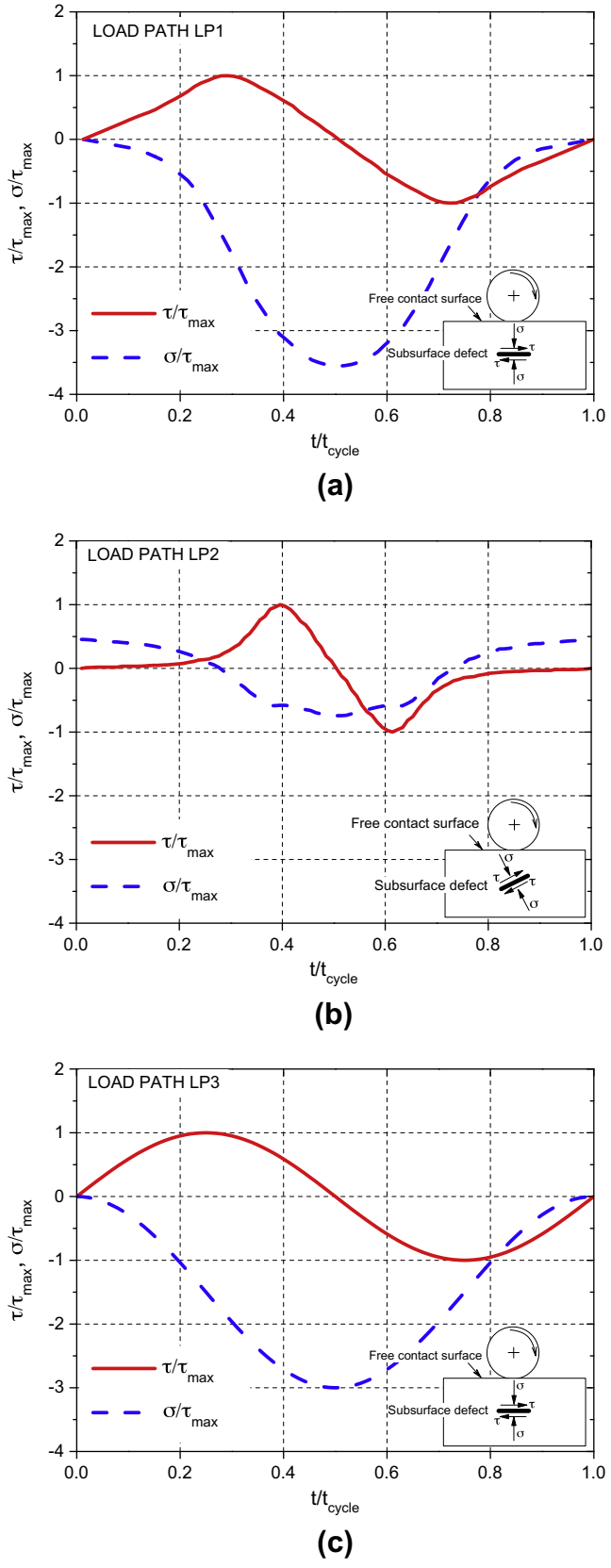

Fig. 2. Load patterns: (a) Load Path 1 (LP1) for bearing steel, (b) Load Path 2 (LP2) for bearing steel and (c) Load Path 3 (LP3) for gear steel and railway wheel steel.

presence of a compressive out-of-phase normal stress, has been studied considering different multiaxial high cycle fatigue criteria.

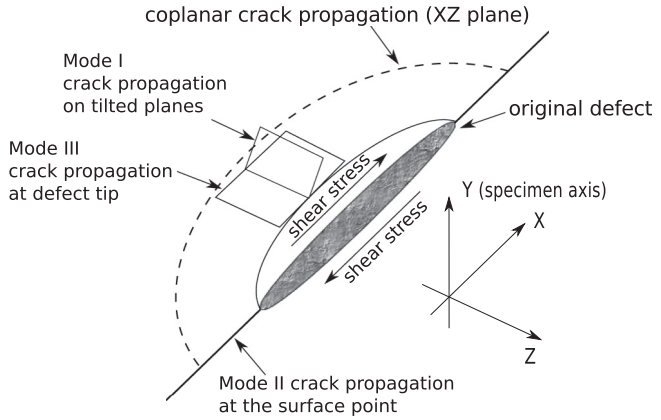

Fig. 3. Schematic illustration of Mode I, II and III crack propagation in multiaxial fatigue tests.

Two different criteria has been selected, i.e. the Dang Van criterion and the Liu–Mahadevan criterion. These two criteria are widely used in literature for the prediction of fatigue life in rolling contact fatigue problems.

For all the materials, a series of axial or bending fatigue tests, at a stress ratio $R = -1$, were carried out on micro-notched and smooth specimens in order to determine the relationship between fatigue strength and defect size (Kitagawa diagram).

The experimental results of the Kitagawa diagram were interpolated by means of the modified El-Haddad model [19]:

$$\sigma_W = \sigma_{W0}\sqrt{\frac{\sqrt{area_0}}{\sqrt{area}+\sqrt{area_0}}} \tag{1}$$

where σ_{W0} is the fatigue limit for smooth specimens, σ_W is the fatigue limit depending on defect size (expressed in terms of Murakami's $\sqrt{area}$ parameter) and $\sqrt{area_0}$ is the fictitious crack length parameter found by interpolating the fatigue limit experimentally obtained for different defect sizes.

The same procedure has been applied to obtain the torsional fatigue limit depending on the defect size. According to the experimental results reported in Refs. [10,11] the ratio s, between the fully reversed torsional fatigue limit, τ_W, and the fully reversed uniaxial fatigue limit, σ_W, is equal to 1 for the bearing and the gear steel. For the railway wheel steel the ratio s is equal to 0.83 as reported in Ref. [4] for smooth specimens. Similar results were also obtained in Ref. [20] with tests onto micronotched specimens.

Due to the confidentiality agreement with the industrial partners involved in this project, all the results presented below will be normalized in respect to the Mode I threshold for long cracks, $\Delta K_{th,I,LC}$, or the axial fatigue limit, σ_W.

3.1. Dang Van fatigue criterion

The basis of the Dang Van criterion is the application of the elastic shakedown principles at the mesoscopic scale (more details can be found in Refs. [13,14]). The Dang Van criterion can be expressed by:

$$\tau_{DV}(t) + \alpha_{DV}\sigma_h(t) \leqslant \tau_W \tag{2}$$

where α_{DV} is a material constant to be determined, τ_W is the fatigue limit in reversed torsion, $\sigma_h(t)$ is the instantaneous hydrostatic component of the stress tensor and $\tau_{DV}(t)$ is the instantaneous value of the Tresca shear stress, that is:

$$\tau_{DV}(t) = \frac{\widehat{s}_I(t) - \widehat{s}_{III}(t)}{2} \tag{3}$$

Table 2
Out-of-phase fatigue test results. Railway wheel steel.

Specimen No.	$\sqrt{area}$ (μm)	$\Delta K_{III}/\Delta K_{I,th,LC}$	Number of cycles	Co-planar Mode III (μm)
R.01	630	0.71	10^5	876
R.06	630	0.59	1.6×10^5	946
R.12	630	0.59	1.6×10^5	957
R.08	630	0.50	2.0×10^5	381
R.09	630	0.50	2.0×10^5	466
R.07	630	0.42	10^6	1741
R.04	630	0.34	10^6	80
R.10	630	0.25	10^6	20
R.24	220	0.71	0.6×10^5	1068
R.18	220	0.59	1.2×10^5	640
R.13	220	0.47	1.2×10^5	241
R.16	220	0.47	1.2×10^5	188
R.19	220	0.36	5.0×10^5	79
R.15	220	0.30	10^6	57

evaluated over a symmetrized stress deviator found at the mesoscopic scale, which is obtained by subtracting from the deviatoric stress $s_{ij}(t)$ a constant tensor, $s_{ij,m}$, that is:

$$\widehat{s}_{ij}(t) = s_{ij}(t) - s_{ij,m} \tag{4}$$

where $s_{ij,m}$ is a residual stress deviator, able to fulfill the condition of an elastic shakedown state at the mesoscopic scale.

The constant α_{DV} appearing in the expression of the Dang Van criterion is usually calibrated with two fatigue tests, that is: tension–compression to determine σ_W and pure torsion to determine τ_W:

$$\alpha_{DV} = 3\left(\frac{\tau_W}{\sigma_W} - \frac{1}{2}\right) \tag{5}$$

The resulting failure locus is a line as reported in the τ_{DV}–σ_h plane (original Dang Van locus in Fig. 6). Plotting onto τ_{DV}–σ_h plane the stress cycles corresponding to a three-dimensional rolling/sliding point contact with a ratio p_0/k_Y equal to 3.5, being p_0 the maximum contact pressure and k_Y the cyclic yield shear stress, Desimone et al. [21] pointed out that, if the conventional Dang Van formulation is considered, failure would not be predicted. On the contrary, the used value of the ratio p_0/k should be the lower limit for fatigue accumulation according to Johnson [22]. In order to predict failure using the Dang Van criterion, Desimone et al. [21] argued that the failure locus in the region with $\sigma_h < 0$ should be modified into a constant value $\tau_W = 0.5\sigma_W$ (proposed conservative locus in Fig. 6). A recent papers [23], with application to bearings, support this kind of modification. The Dang Van criterion, in its original and modified forms, is then applied to experimental data previously discussed.

3.1.1. Bearing steel

The application of the Dang Van criterion to the bearing steel for LP1 is reported in Fig. 7. The results are normalized with respect to the axial fatigue limit, σ_W. For each defect size, three different fatigue tests are reported in the Dang Van plane (τ_{DV} versus σ_h): the first one, characterized by the lower value of the ratio $\Delta K_I/\Delta K_{I,th,LC}$, equal to 0.3 for $\sqrt{area} = 220$ μm and 0.49 for $\sqrt{area} = 630$ μm, is below the out of phase fatigue limit with the presence of non-propagating cracks; the second one, with a ratio $\Delta K_{III}/\Delta K_{I,th,LC}$ equal to 0.38 for $\sqrt{area} = 220$ μm and 0.53 for $\sqrt{area} = 630$ μm, is a middle value with an initial coplanar crack growth; finally the last one, with a ratio $\Delta K_{III}/\Delta K_{I,th,LC}$ equal to 0.62 for $\sqrt{area} = 220$ μm and 0.68 for $\sqrt{area} = 630$ μm, is characterized by a evident coplanar crack growth. Despite the evident coplanar crack growth, all the fatigue tests are below the original locus proposed by Dang Van. Hence, it is possible to conclude that, at least for a coplanar/Mode III failure, the original Dang Van criterion is not able to correctly predict the experimental results, leading to unsafe predictions.

The introduction of a new conservative locus, as proposed by Desimone et al. in Ref. [21], seems to better reproduce the experimental results. For the smaller defect size (Fig. 7-a), the fatigue limit in out-of-phase is correctly predicted. This tendency is confirmed by the second defect size, even if the prediction seems to be a little more conservative.

The introduction of the conservative locus seems to be a necessary condition for the prediction of Mode III failure: as a matter of fact, the out-of-phase tests have clearly shown this is a failure mode completely different from the 'usual' Mode I that defines the original Dang-Van locus (which is defined by fatigue limits under tension–compression and torsion). So the superposition of a more conservative limit appears to be correct. It is also important to note that Mode I crack propagation never appears in LP1 fatigue tests, if the load path in the Dang Van plane is below the original locus. This can be noted in Fig. 8a, where two different fatigue tests are reported. The first one, characterized by a ratio of $\Delta K_{III}/\Delta K_{I,th,LC}$ equal to 0.62, is below the original Dang Van locus and no evidence of mode I crack propagation has been experimentally observed. On the contrary, as soon as the loading path in the Dang Van plane exceeds the original locus, it is always possible to observe on the specimen surface the formation of a Mode I crack, confirming the idea that this original locus can be seen as a Mode I failure locus.

This idea apparently looks to be supported by the analysis of LP2 and torsional tests. Since, failure under these tests is controlled by Mode I, drawing all these load paths in the Dang Van plane, it is possible to observed that in all cases the Mode I failure is characterized by the crossing of the original locus, as reported in Fig. 8b.

3.1.2. Gear steel and railway wheel steel

The results obtained for the gear and railway wheel steels under torsion and LP3 are very similar to the ones of the bearing steel. In particular, torsional fatigue limit corresponds to the onset of Mode I propagation onto tilted planes, while OOP tests show a threshold ΔK_{III} much lower than $\Delta K_{I,th}$. The predictive capabilities of the Dang Van criterion have been checked for these two steels. In Fig. 9 the experimental results are reported in the Dang Van plane for the railway wheel steel. The results confirm the same trend previously discussed for the bearing steel. The original Dang Van locus fails in the prediction of a Mode III crack growth, while the proposed conservative locus is able to correctly predict the multiaxial fatigue limit in out-of-phase.

3.2. Liu–Mahadevan fatigue criterion

The Liu–Mahadevan criterion [15,16] is a high cycle fatigue criterion based on the definition of a critical plane and a fatigue

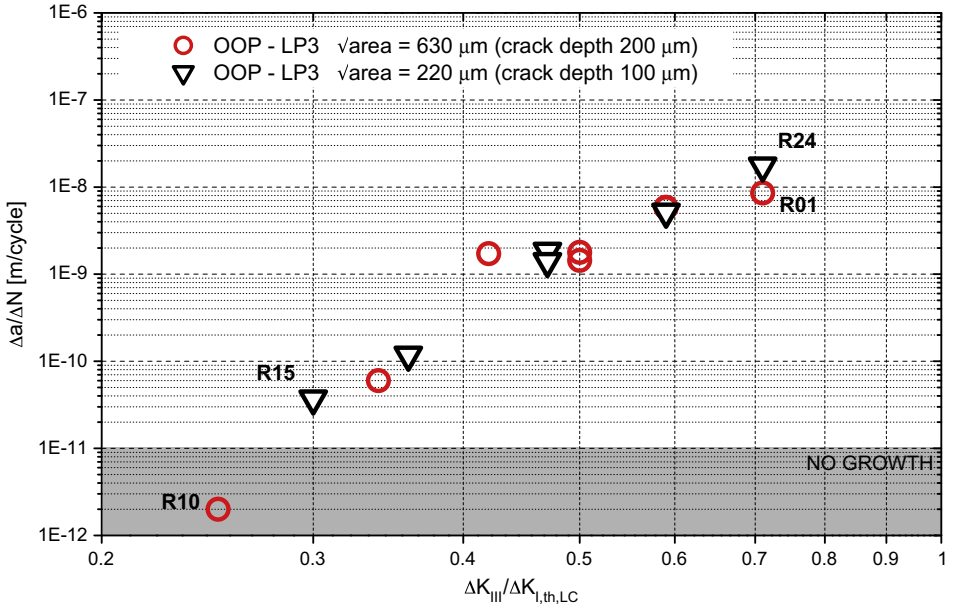

R15: Coplanar crack depth a = 57 μm, N = 10^6 cycles

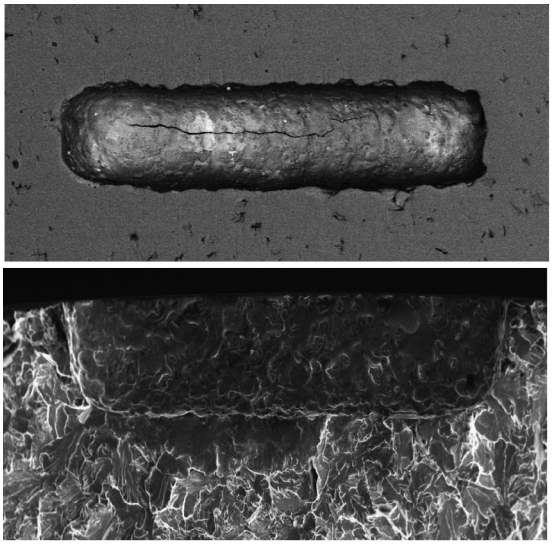

R24: Coplanar crack depth a = 1068 μm, N = $0.6x10^5$ cycles

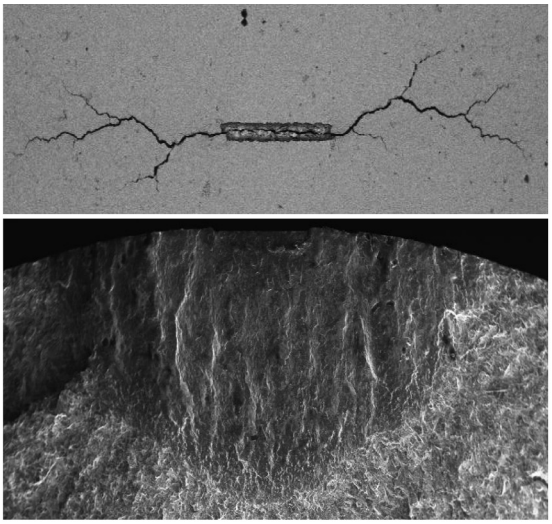

R01: Coplanar crack depth a = 876 μm, N = 10^5 cycles

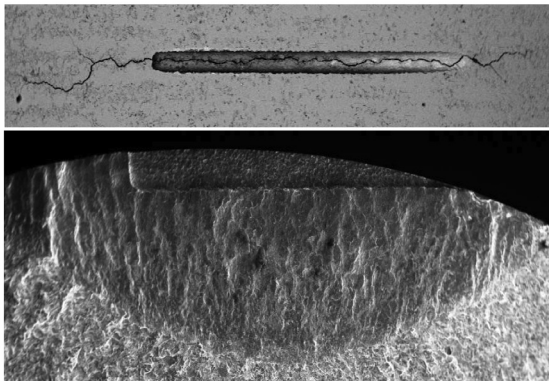

R10: Coplanar crack depth a = 20 μm, N = 10^6 cycles

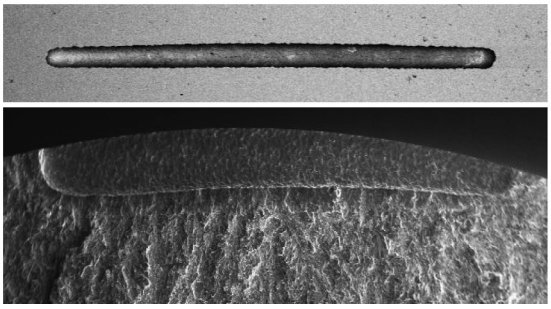

Fig. 4. Coplanar Mode III averaged propagation rates under out-of-phase fatigue tests for the railway wheel steel tested.

fracture plane, where the fracture plane is the crack plane observed at macro level, while the critical plane is a material plane where the fatigue damage is evaluated. In the original proposed model the fracture plane is defined as the plane which experiences the maximum normal stress amplitude.

The critical plane orientation may differ from the fatigue fracture plane for different materials [15]. For extremely brittle materials, characterized by a ratio between the fully reversed torsional fatigue limit and the fully reversed uniaxial fatigue limit $s \geqslant 1$, the value of the angle α between the fracture plane and the critical

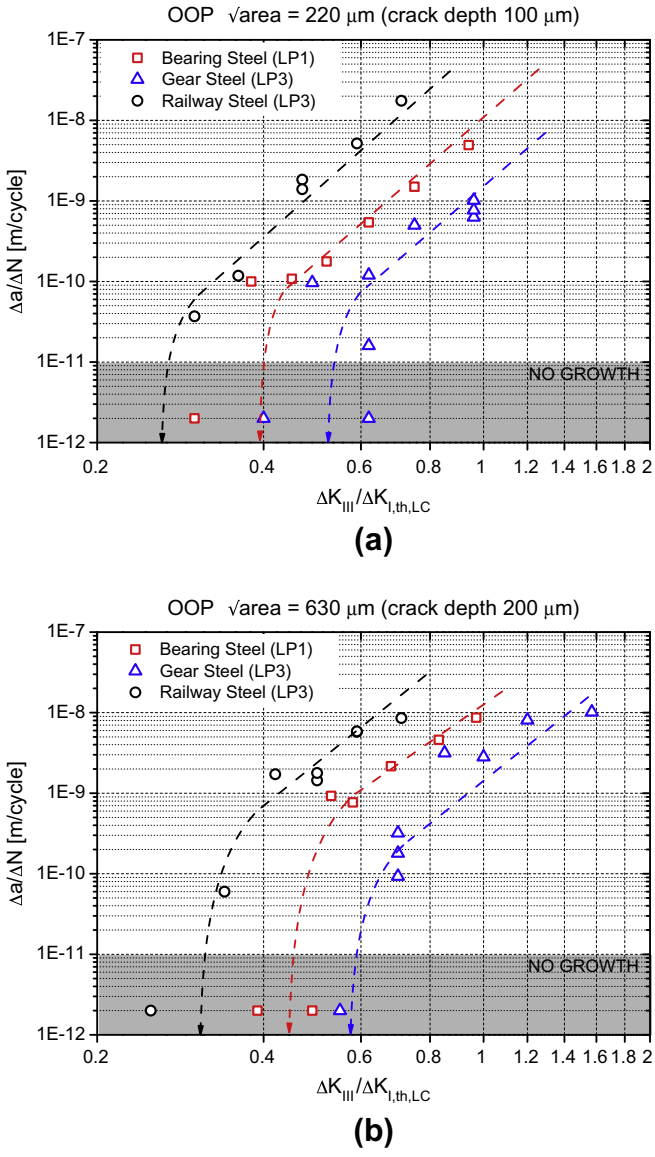

Fig. 5. Coplanar Mode III crack growth rate versus mode III stress intensity factor range under out-of phase fatigue tests. Comparison between the different tested materials: defect size equal to $\sqrt{\text{area}} = 220$ μm (a) and $\sqrt{\text{area}} = 630$ μm (b).

plane can be set to zero, so that the critical plane coincides with the fracture plane. In the general case the angle α can be obtained as a function of the ratio s:

$$\cos(2\alpha) = \frac{-2 + \sqrt{4 - 4(1/s^2 - 3)(5 - 1/s^2 - 4s^2)}}{2(5 - 1/s^2 - 4s^2)} \tag{6}$$

Once the critical plane has been defined, the fatigue model is:

$$\sigma_{eq} = \frac{1}{\beta}\sqrt{\left[\sigma_{a,c}\left(1 + \eta\frac{\sigma_{m,c}}{\sigma_W}\right)\right]^2 + \left(\frac{\sigma_W}{\tau_W}\right)^2 (\tau_{a,c})^2 + k\left(\sigma^H_{a,c}\right)^2} \tag{7}$$

where $\sigma_{a,c}$, $\tau_{a,c}$ and $\sigma^h_{a,c}$ are the normal stress amplitude, shear stress amplitude and hydrostatic stress amplitude acting on the critical plane respectively. $\sigma_{m,c}$ is the mean normal stress acting on the critical plane. β, η, and k are material parameters depending on the ratio, s, between the torsional and the uniaxial fully reversed fatigue limit:

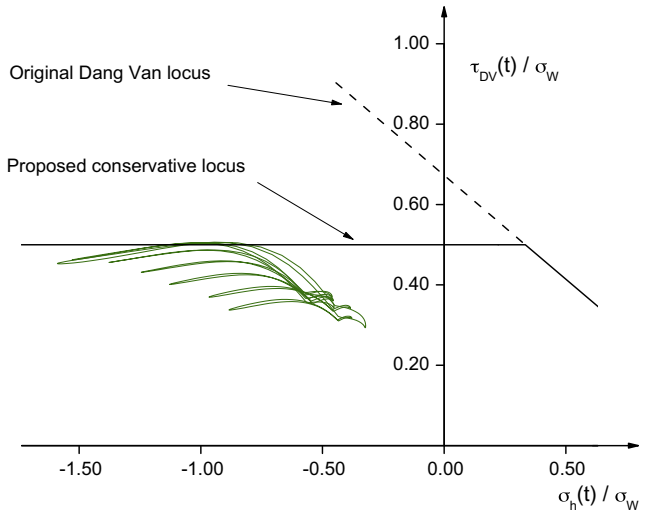

Fig. 6. Definition of the proposed conservative locus for the Dang Van criterion. Application of Dang Van criterion to rolling/sliding contact, for a spherical contact of radius 1 mm and friction coefficient $\mu = 0.1$.

$$s = \frac{\tau_W}{\sigma_W} \geqslant 1 \Rightarrow \begin{cases} \beta = s \\ k = 9(s^2 - 1) \\ \eta = 1 \end{cases} \tag{8}$$

$$s = \frac{\tau_W}{\sigma_W} < 1 \Rightarrow \begin{cases} \beta = \sqrt{\cos^2(2\alpha)s^2 + \sin^2(2\alpha)} \\ k = 0 \\ \eta = \frac{3}{4} + \frac{1}{4}\left(\frac{\sqrt{3} - 1/s}{\sqrt{3} - 1}\right) \end{cases} \tag{9}$$

3.2.1. Bearing steel

The application of the Liu–Mahadevan criterion to the bearing steel is shown in Fig. 10. The results are normalized in respect to the axial fatigue limit, σ_W. The application of this criterion to the LP1 gives good results. The prediction of the fatigue limit is correct for a defect size equal to $\sqrt{\text{area}} = 630$ μm. On the contrary, the prediction in the case of a defect size equal to $\sqrt{\text{area}} = 220$ μm seems to be slightly non-conservative. The predicted fracture plane for LP1, the horizontal plane, is in full agreement with the observed macroscopic crack plane.

For the LP2 the prediction of the Liu–Mahadevan criterion is still good (Fig. 10-c). The predicted fracture plane inclined by an angle of 50° with respect to the horizontal direction, is also in good agreement with experimentally observed macroscopic fracture plane.

3.2.2. Gear steel and railway wheel steel

The good predictions showed by the Liu–Mahadevan criterion are fully confirmed by its application to the gear steel in the prediction of both the fatigue limit and the fracture plane.

A different conclusion has to be drawn for the railway steel. The application of the Liu–Mahadevan criterion gives non-conservative results in the case of defect size equal to $\sqrt{\text{area}} = 630$ μm (Fig. 11). For a fatigue tests characterized by a huge coplanar crack depth, greater than 1.7 mm in 10^6 cycles, the equivalent stress predicted by the Liu–Mahadevan criterion is still well beneath the fatigue limit.

As a result, to obtain an equivalent stress equal to the fatigue limit is required to apply a $\Delta K_{III,OOP}$ in out-of-phase tests equal to 0.65 the Mode I threshold for long crack, a value well greater than the experimental one, estimated in the range 0.35–0.40.

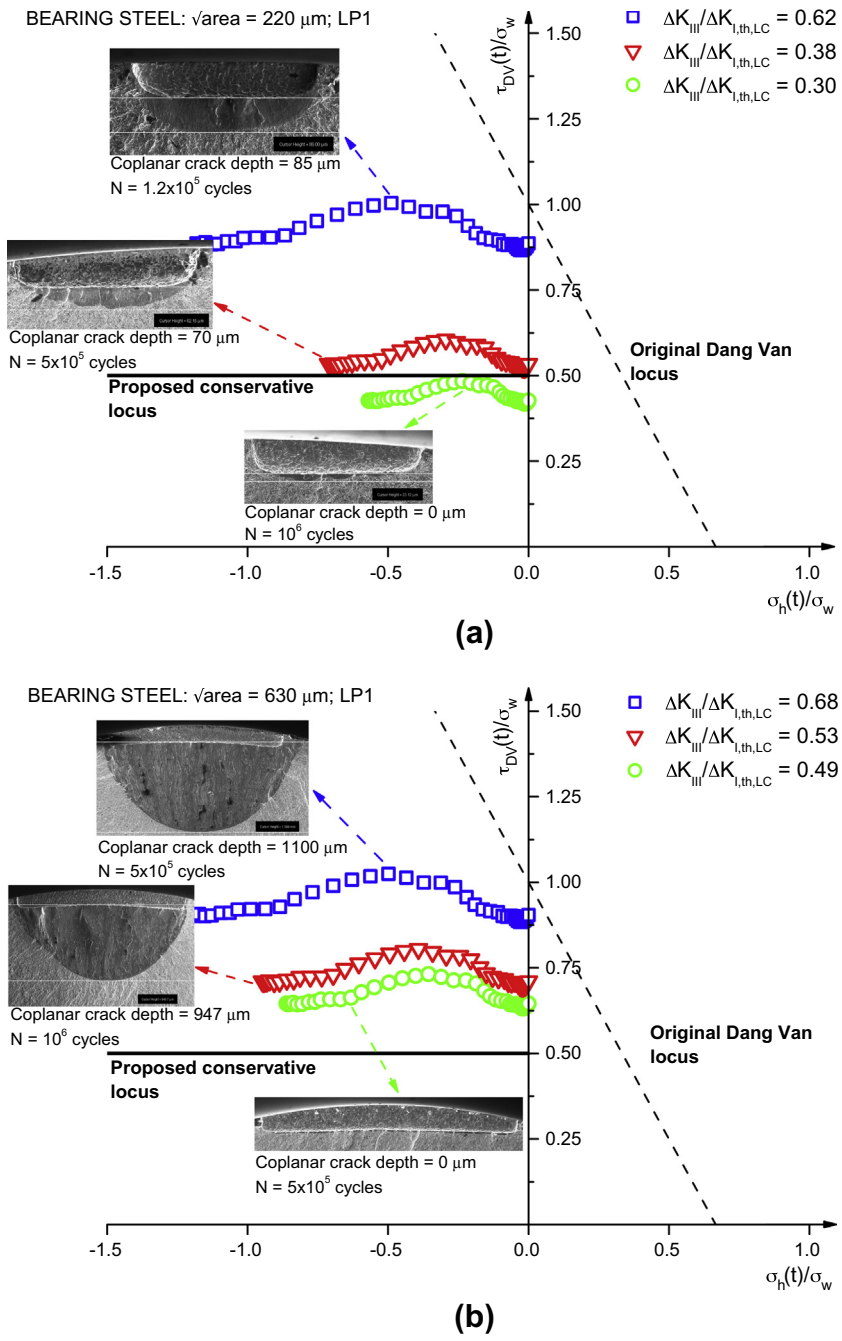

Fig. 7. Application of Dang Van criterion to bearing steel and Load Path 1: defect size equal to $\sqrt{area}$ = 220 μm (a) and $\sqrt{area}$ = 630 μm (b).

4. Discussion

Different criteria have been compared in their capability to correctly predict the Mode III threshold under rolling contact fatigue condition. In Fig. 12 is reported the application of the different criteria to bearing steel experimental results with a defect size equal to $\sqrt{area}$ = 220 μm. The vertical grey band represents the Mode III threshold experimentally obtained in OOP tests. The horizontal line represents the condition for the crack growth predicted by the different criteria. For the Dang Van criterion, the equivalent stress is the equivalent shear stress obtained as the maximum value over the observation time (Eq. (2)). For the Liu–Mahadevan criterion the equivalent stress is the value obtained by applying Eq. (7). The predicted Mode III threshold can be calculated as the intersection between the prediction of the different criteria for different applied loads (different value of the ratio $\Delta K_{III}/\Delta K_{I,th,LC}$ in Fig. 12) and the horizontal line. As reported in Fig. 12 the Dang Van criterion with the original locus gives a very non-conservative prediction. On the contrary, changing the definition of the failure locus, the prediction becomes conservative. The best prediction is achieved by the application of the Liu–Mahadevan criterion.

The same conclusions are still valid for the other materials and for the other defect sizes. The results are reported in Table 3.

The biggest error in the application of the Liu–Mahadevan criterion is achieved in the case of the railway wheel steel. This result is strongly influenced by the ratio *s*. The results reported in Table 3

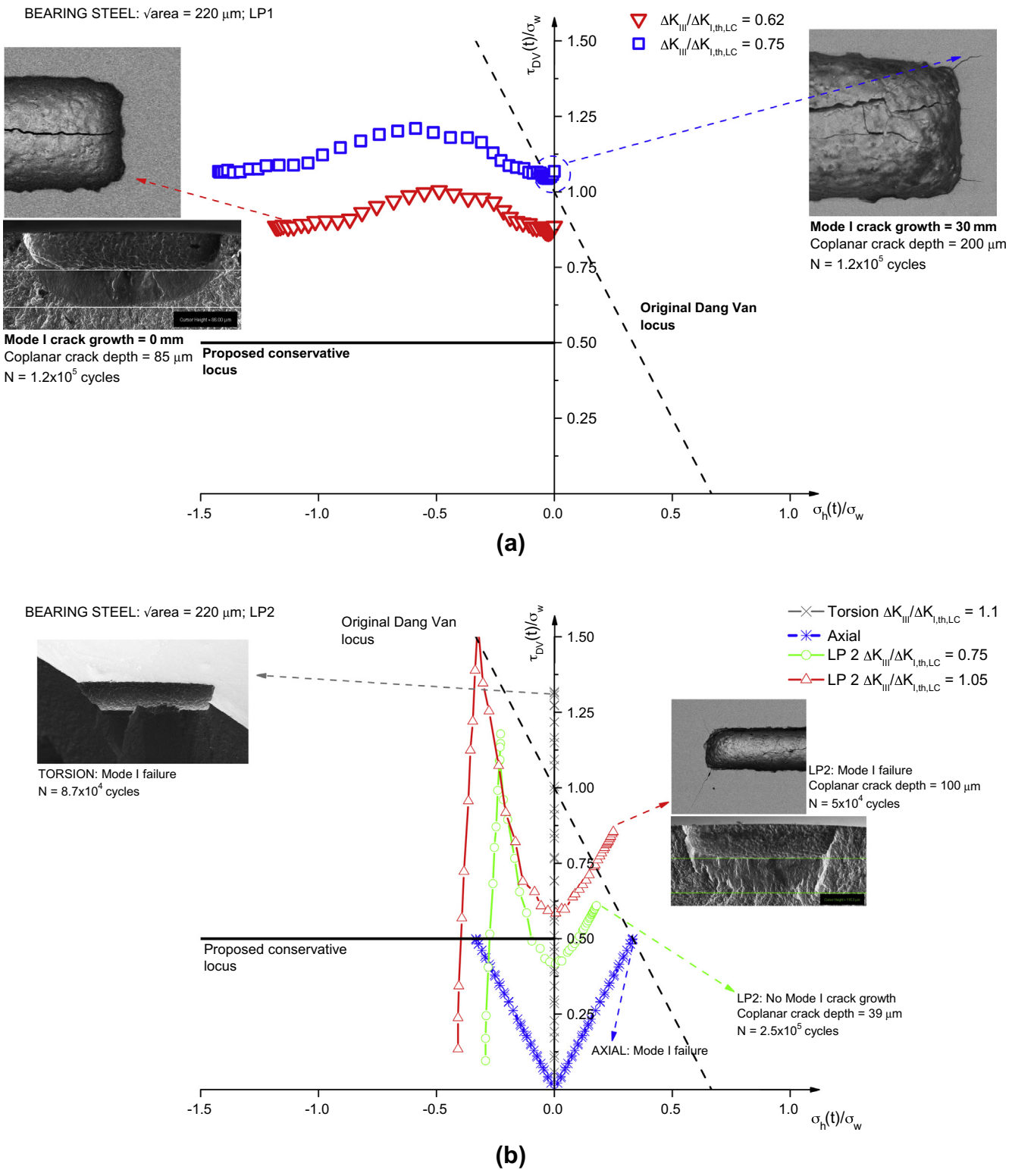

Fig. 8. Mode I and Mode III crack propagation in the Dang Van plane. Bearing steel with defect size equal to $\sqrt{area}$ = 220 μm: Load Path 1 (a) and Load Path 2 (b).

have been obtained using a ratio *s*, in agreement with the experimental results, equal to 0.83. This ratio is typical of materials containing defects, but it is not a typical value of a ductile material. Changing the *s* value in the Liu–Mahadevan criterion, the predicted Mode III threshold in rolling contact fatigue conditions changes approaching the experimental value, as can be observed in Fig. 13. A value of the *s* ratio equal to 0.5 fulfills the experimental threshold in mode III under the out-of-phase scheme. The results of the Liu–Mahadevan criterion as a function of the ratio *s* are reported in Table 4.

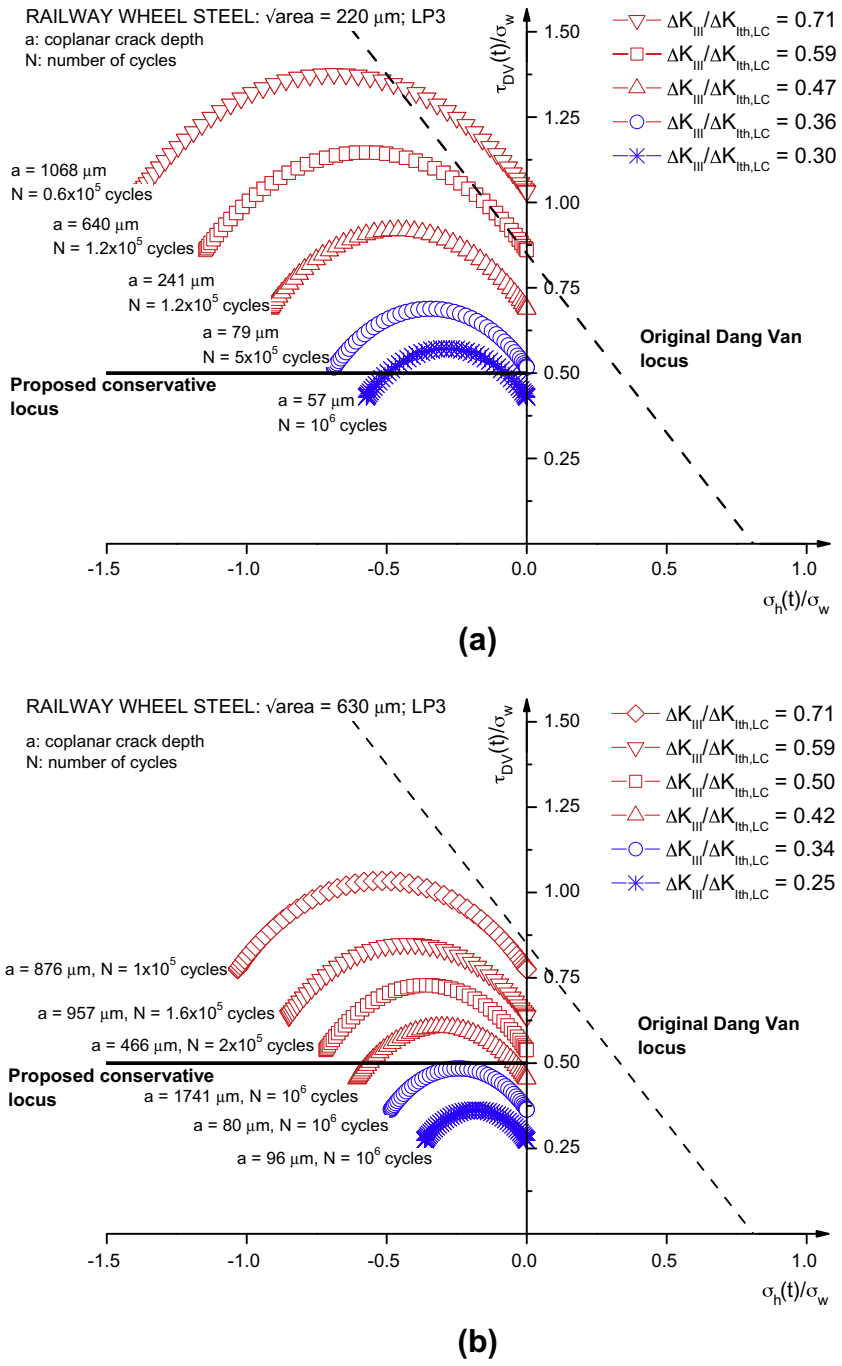

Fig. 9. Application of Dang Van Criterion to railway wheel steel and Load Path 3: defect size equal to $\sqrt{area}$ = 220 μm (a) and $\sqrt{area}$ = 630 μm (b).

5. Conclusions

In this paper we summarize the fatigue test results obtained for three different steels (a bearing, a gear and a railway wheel steels) that have been subjected to out-of-phase multiaxial fatigue tests, simulating RCF conditions in presence of small shallow pre-cracks. The experimental results have then been discussed adopting the Dang Van criterion and the Liu–Mahadevan criterion, that are two multiaxial high cycle fatigue criteria widely adopted for fatigue analysis in contacting bodies.

The results show that the fatigue resistance domain is characterized by the presence of two different phenomena. In the region of $\sigma_h < 0$, tests simulating RCF for deep defects show a peculiar co-planar propagation driven by shear, while in torsional tests and out-of-phase tests with $\sigma_h > 0$, the fatigue strength appears to be controlled by the onset of Mode I propagation.

The Dang Van criterion with the original failure locus is not able to predict both failure mechanisms. The original locus seems to correspond to Mode I failure experimentally observed in torsional fatigue tests and in the Loading Path 2 for the bearing steel. On the contrary, the application of the original failure locus is extremely non-conservative in the prediction of Mode III failure experimentally observed in out-of-phase fatigue tests. These results have been confirmed on three different materials with different cyclic and monotonic properties, from extremely brittle to ductile steels. The introduction of a different failure locus, characterized by the

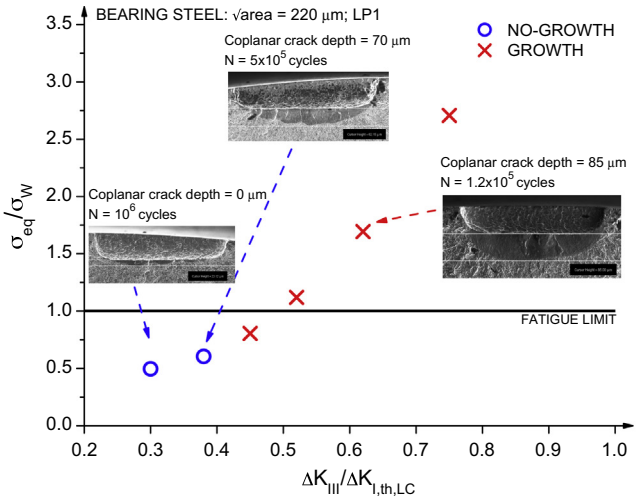

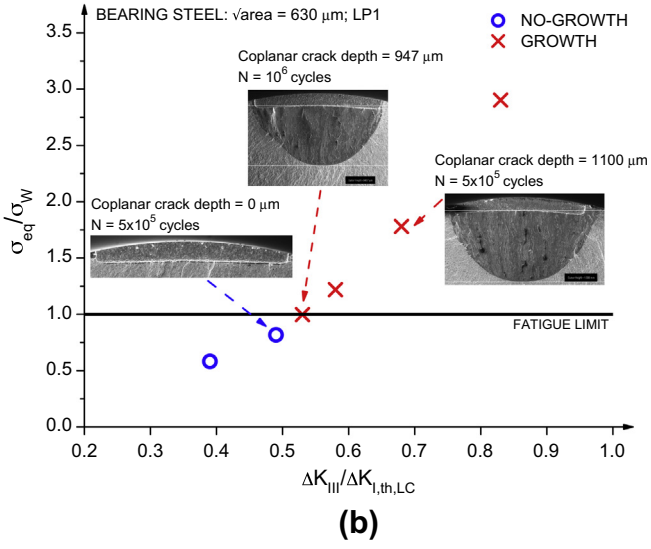

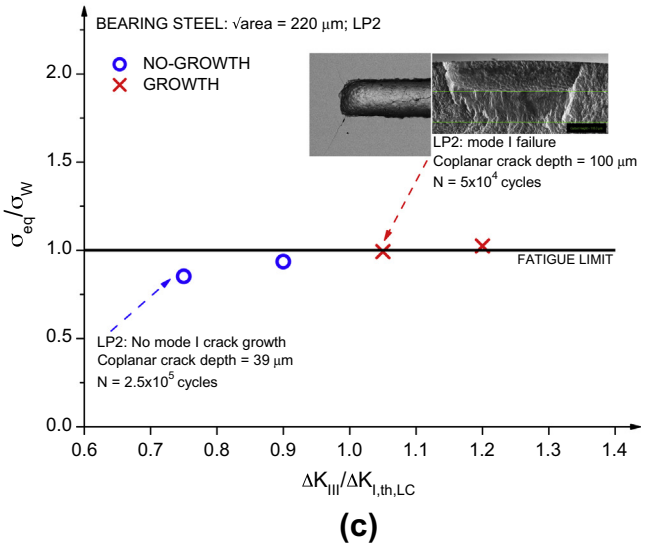

Fig. 10. Application of Liu–Mahadevan criterion. Bearing steel, Load Path 1, defect size equal to $\sqrt{area}$ = 220 μm (a) and $\sqrt{area}$ = 630 μm (b). Bearing steel, Load Path 2 and defect size equal to $\sqrt{area}$ = 220 μm (c).

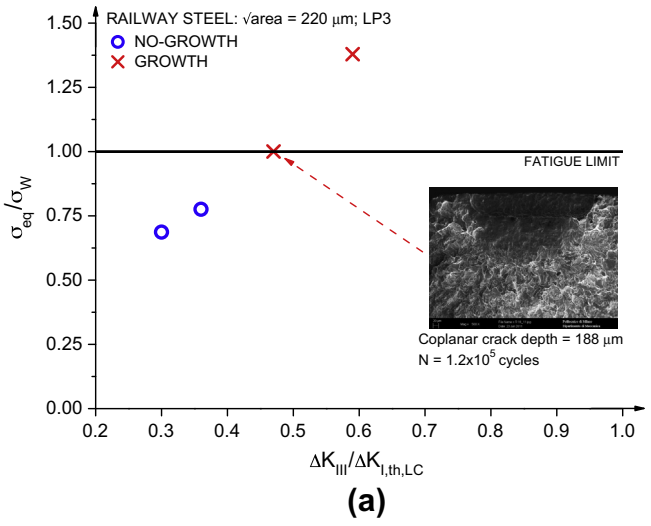

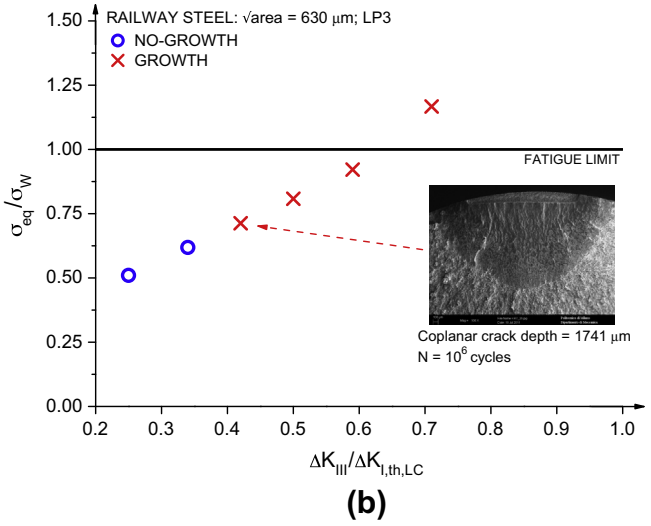

Fig. 11. Application of Liu–Mahadevan criterion. Railway wheel steel, Load Path 3 and defect size equal to $\sqrt{area}$ = 220 μm (a) and $\sqrt{area}$ = 630 μm (b).

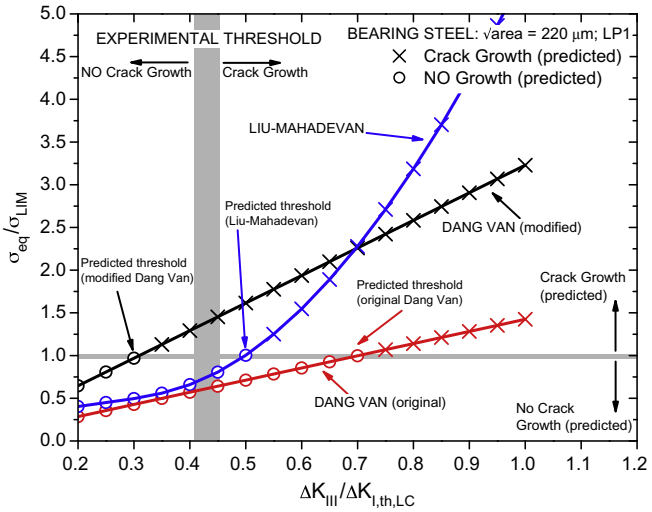

Fig. 12. Comparison between multiaxial fatigue criteria. Bearing steel, Load Path 1 and defect size equal to $\sqrt{area}$ = 220 μm.

Table 3
Mode III threshold under out-of-phase fatigue tests in term of the ratio $\Delta K_{III,th,OOP}/\Delta K_{I,th,LC}$, evaluated by employing the experimental value of the s ratio.

Material	$\sqrt{area}$ (μm)	Experimental	Original Dang Van	Modified Dang Van	Liu–Mahadevan
Bearing steel	630	0.45–0.50	0.75	0.33	0.53
Bearing steel	220	0.40–0.45	0.70	0.32	0.50
Gear steel	630	0.60–0.65	0.92	0.35	0.62
Gear steel	220	0.55–0.60	0.98	0.37	0.65
Railway wheel steel	630	0.35–0.40	0.78	0.35	0.63
Railway wheel steel	220	0.30–0.35	0.58	0.26	0.47

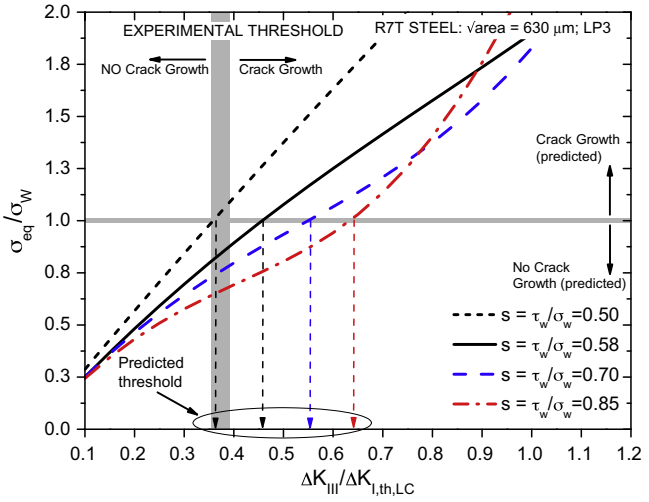

Fig. 13. Effect of the ratio s on the prediction of Liu–Mahadevan criterion. Railway wheel steel, Load Path 1 and defect size equal to $\sqrt{area}$ = 630 μm.

Table 4
Influence of the s ratio on the mode III threshold under out of phase fatigue tests, in term of the ratio $\Delta K_{III,th,OOP}/\Delta K_{I,th,LC}$, for the railway wheel steel using the Liu–Mahadevan criterion.

$\sqrt{area}$ (μm)	Experimental	s = 0.5	s = 0.58	s = 0.83
630	0.35–0.40	0.36	0.46	0.63
220	0.30–0.35	0.27	0.34	0.47

independence of fatigue limit by hydrostatic stress for negative values, seems to underestimate the Mode III failures under OOP tests.

The Liu–Mahadevan criterion is able to discern between brittle and ductile steels by the definition of a different set of material parameters. For the brittle steels, i.e. the bearing and the gear steels, characterized by a ratio s between the torsional and the uniaxial fatigue limit equal to 1, the Liu–Mahadevan criterion is able to give good predictions for both Mode I and Mode III failure mechanism. The application to ductile steel, i.e. the railway wheel steel, gives non-conservative results. However, predictions due to Liu–Mahadevan can become very precise if the ratio s is fixed to 0.5 (typical for ductile steels) instead of considering the experimental one.

References

[1] Harris TA, Kotzalas MN. Rolling bearing analysis. Boca Raton (FL): CRC Press; 2007.
[2] Dang Van K, Cailletaud G, Flavenot JF, Le A, Douaron HP, Lieurade. Criterion for high cycle fatigue failure under multiaxial loading. In: Biaxial and Multiaxial Fatigue . Mechanical Engineering Publications, London; p. 459–478 1989.
[3] Ekberg A, Kabo E, Andersson H. An engineering model for of rolling contact fatigue for railway wheels. Fatigue Fract Eng Mater Struct 2002;25:899–909.
[4] Bernasconi A, Davoli P, Filippini M, Foletti S. An integrated approach to rolling contact sub-surface fatigue assessment of railway wheels. Wear 2005;258:973–80.
[5] Sandstrom J. Subsurface rolling contact fatigue damage of railway wheels – A probabilistic analysis. Int J Fatigue 2012;37:146–52.
[6] Gullers P, Dreik P, Nielsen JCO. Ekberg A, Andersson L, Track condition analyser: identification of rail rolling surface defects, likely to generate fatigue damage in wheels, Using instrumented wheelset measurements. In: Proceedings of the institution of mechanical engineers. vol. 225. Part F: J Rail and Rapid Transit; 2011. p. 1–13.
[7] Donzella G, Petrogalli C. A failure assessment diagram for components subjected to rolling contact loading. Int J Fatigue 2010;32. 256–268.
[8] Ekberg A, Kabo E, Nielsen JCO, Lunden R. Subsurface initiated rolling contact fatigue of railway wheels as generated by rail corrugation. Int J Solids Struct 2007;44:7975–87.
[9] Murakami Y. Metal fatigue: effects of small defects and nonmetallic inclusions. Oxford: Elsevier; 2002.
[10] Beretta S, Foletti S, Valiullin K. Fatigue crack propagation and threshold under out- of-phase multiaxial loading in a gear steel. Eng Fract Mech 2010;77:1835–48.
[11] Tarantino MG, Beretta S, Foletti S, Lai J. A comparison of Mode III threshold under simple shear and RCF conditions. Eng Fract Mech 2011;78:1742–55.
[12] Desimone H, Bernasconi A, Beretta S. Are multiaxial fatigue criteria appropriate when steels with surface defects are subjected to RCF? J ASTM Int 2006;3:1–7.
[13] Dang Van K. Macro–micro approach in high-cycle multiaxial fatigue. In: McDowell DL, Ellis R, editors. Advances in Multiaxial Fatigue, ASTM STP 1191, Philadelphia; 1993. p. 120–130
[14] Dang Van K, Griveau B, Message O. On a new multiaxial fatigue limit criterion: theory and applications. In: Brown MW, Miller KJ, editors. EGF 3. London: Mechanical Engineering Publications; 1989. p. 479–96.
[15] Liu Y, Mahadevan S. Multiaxial high-cycle fatigue criterion and life prediction for metals. Int J Fatigue 2005;27:790–800.
[16] Liu Y, Stratman B, Mahadevan S. Fatigue crack initiation life prediction of railroad wheels. Int J Fatigue 2006;28:747–56.
[17] Tarantino MG, Beretta S, Foletti S, Papadopoulos I. Experiments under pure shear and rolling contact fatigue conditions: competition between tensile and shear mode crack growth. Int J Fatigue 2013;46:67–80.
[18] Tarantino MG. Shear mode propagation of short cracks under rolling contact fatigue, Ph. D thesis, Politecnico di Milano; 2011.
[19] Beretta S. Propagation of short cracks in a high strength steel for railway axles. In: Proc European Conference on Fracture ECF14, Krakow; 2002.
[20] Beretta S, Donzella G, Roberti R, Ghidini A. Deep shelling in railway wheels. In: Proceedings 13th international wheelset congress, Rome, Italy; 2001.
[21] Desimone H, Bernasconi A, Beretta S. On the application of Dang Van criterion to rolling contact fatigue. Wear 2006;260:567–72.
[22] Ponter A, Hearle A, Johnson K. Application of the kinematical shakedown theorem to rolling and sliding point contacts. J Mech Phys Solids 1984;33:339–64.
[23] Houpert L, Chevalier F. Rolling bearing stress based life – Part 1: calculation model. J Tribol 2012:134.